Polymer Bulletin 61, 725–736 (2008)
DOI 10.1007/s00289-008-1004-9

Polymer Bulletin

Synthesis and aggregate formation of poly(styrenesulfonate)-*b*-poly(ethylene glycol)-*b*-poly(styrenesulfonate) triblock copolymers in aqueous solution induced by binding with aluminum ions

Zhiping Peng, Xinxing Liu, Zhen Tong (✉)

Research Institute of Materials Science, South China University of Technology, Guangzhou 510640, China
E-mail: mcztong@scut.edu.cn; Fax: (86)-20-87112886-602

Received: 17 July 2008 / Revised version: 11 September 2008 / Accepted: 12 September 2008
Published online: 26 September 2008 –

Summary

Well-defined water-soluble poly(styrenesulfonate)-*b*-poly(ethylene glycol)-*b*-poly(styrenesulfonate) (PSS-*b*-PEG-*b*-PSS) triblock copolymers with narrow molecular weight distribution ($1.29 < M_w/M_n < 1.36$) were synthesized in aqueous solution at 70°C via reversible addition-fragmentation chain transfer (RAFT) polymerization. The complex formed by the PSS-*b*-PEG-*b*-PSS triblock copolymer coordinated with aluminum ion was investigated with turbidimetry, dynamic light scattering (DSL), zeta-potential, and transmission electron microscopy (TEM). The aggregation formation was based on the neutralization of the SO_3^- groups in the PSS blocks with Al^{3+} ions. The appearance, size and stability of the PSS-*b*-PEG-*b*-PSS/Al^{3+} aggregates were controlled by varying the PSS block length and degree of neutralization (DN). At DN = 0.33, where the PSS-*b*-PEG-*b*-PSS copolymer was completely neutralized with Al^{3+}, the aggregate size increased with increasing PSS block length. The transition from the shrinking coil of small size to the interchain aggregates of large size was found at DN of about 0.33.

Introduction

Water-soluble block copolymers with charged groups on the chain have received considerable attention during recent years for various current and potential applications in gene delivery and therapy [1-3], drug encapsulation and release [4-6], crystal growth modifier and mineralization template [7-11], and synthesized nanoparticale [12-14].] The ionizible blocks in these copolymers can be converted to hydrophobic blocks due to neutralization of the charge with oppositely charged species, such as counterions, surfactants, and polyelectrolytes to produce micelles, nanoparticles, colloids, and other aggregates [15].

Bronstein et al. reported the micelle formation from poly(ethylene oxide)-polyethyleneimine block copolymer (PEO-*b*-PEI) coordinated with some compounds of Pd, Au, and Pt in water [14]. The polydispersity, stability, shape and size of these micelles were adjusted with species of the metal compounds, the mole ratio of metal ions to charged groups of polymer, and type of the reducing agents. Li et al. prepared

micelle-like nano-aggregates with a neutralized polyion core and a surround PEO corona by complexation of the poly(ethylene oxide)-poly(methacrylate acid) copolymer (PEO-*b*-PMAA) with alkaline-earth metal ions [16]. They also demonstrated formation of the PEO-*b*-PMAA nano-aggregates through binding with cationic anesthetics [17]. The property of these aggregates strongly depended on the hydrophobicity of the anesthetic and the hydrophobic interaction between the PMAA block and anesthetic. Kataoka et al. prepared the polymer-metal complex micelles containing anti-tumor active *cis*-diamindichloroplatinum (II) in the core for the purpose of cancer targeting drug delivery. These micelles were formed by the poly(ethylene glycol)-*b*-poly(*α,β*-aspartic acid) diblock copolymer (PEG-*b*-P(Asp)) coordinated with platinum ions(II) in aqueous medium [18,19]. Core-shell complex micelles were also fabricated by the electrostatic interaction between the cationic lysozyme and PEG-*b*-P(Asp), and then the lysozyme was entrapped in the core and segregated from the surrounding environment by the PEG corona [20,21]. The on-off switch of the enzyme activity was achieved by the reversible micellization of lysozyme with PEG-*b*-P(Asp) through changing the ionic strength [22]. Therefore, the ionic compound can be encapsulated in the core and this technique demonstrated potential applications in ionic drug delivery, nanoreator for colloid synthesis, and novel organic-inorganic hybrids [16-20]. However, PMAA and P(Asp) are weak polyacids and only partially ionized in water. The aggregation behavior of these block copolymers binding with oppositely charged species depended strongly on the solution pH.

Poly(styrenesulfonate) (PSS) is a strong and typical flexible polyelectrolyte which has widely used in the research of polyelectroyte-counterion interaction [23-25]. The strongly attractive interaction between multivalent counterions and monovalent sulfonate group (SO_3^-) on the PSS chain results in the change of PSS conformation. The properties of solution associated with PSS-counterion interaction are dependent on the counterion valency, counterion size, SO_3^- concentration and the molecular weight of PSS [23, 24]. When trivalent salt ($AlCl_3$ or $GaCl_3$) was added to the PSS solution, the PSS chain collapse to a more compact state for the ionic bridging between the trivalent counterion (Al^{3+} or Ga^{3+}) and SO_3^-. The PSS chain undergoes precipitation and redissolution for the competition of ionic bridging between intramolecular and intermolecular when further addition of $AlCl_3$ or $GaCl_3$ [23, 25]. We found that the aggregation formed when $AlCl_3$ was added to the solution of water-soluble copolymers containing PSS block.

The purpose of the present work was to study the influence of charged block length and degree of neutralization (DN) on the aggregate behavior of the water-soluble copolymers. Well-defined structure PSS-*b*-PEG-*b*-PSS triblock copolymers with narrow molecular weight distribution (M_w/M_n = 1.29~1.36) were synthesized via. reversible addition fragmentation chain transfer (RAFT) polymerization. The aggregate behavior of the PSS-*b*-PEG-*b*-PSS copolymers induced by binding with aluminum ions was observed with turbidity, *ζ*-potential, dynamic light scattering, and TEM and discussed in terms of the PSS block length and DN.

Experimental Part

Materials

The PEG-based RAFT macromolecular chain transfer agent (PEG macro-CTA, M_n = 4900, M_w/M_n = 1.02, $M_{n,NMR}$ = 4550) containing 4-cyanopentanoic acid dithiobenzoate

end groups was synthesized following the procedure reported previously [26]. 4,4'-Azobis(4-cyanopentanoic acid) (ACPA, Fluka, 98.0%) was recrystallized from methanol. Sodium 4-styrenesulfonate (NaSS, Fluka, 90%) was dried under vacuum at 40°C for 24 h. Aluminum chloride of analysis grade reagent was used for neutralizing PSS blocks without further purification. Water was purified with a Milli-Q purification system after distillation.

Synthesis of PSS-b-PEG-b-PSS Triblock Copolymers

The PSS-*b*-PEG-*b*-PSS triblock copolymers were synthesized in aqueous solution at 70°C via. the RAFT polymerization. PEG macro-CTA capped with 4-cyanopentanoic acid dithiobenzoate end groups and ACPA were used as the CTA and initiator, respectively. As a typical experiment, a 50 mL round-bottom flask was charged with PEG macro-CTA (0.55 g, 0.12 mmol), NaSS (3.45 g, 15.0 mmol), and ACPA (15 mg, 0.048 mmol) in deionized water (7.5 mL, $[NaSS]_0 = 2.0$ mol/L, $[NaSS]_0/[CTA]_0 = 125$). Three freezing-pump-thaw cycles were performed to remove oxygen from the polymerization solution. After degassing, the flask was tightly sealed under vacuum and heated in an oil bath at 70°C for 5 h. The length of PSS block was adjusted by controlling the amount of NaSS monomer. The reaction was terminated with rapid cooling and freezing. The copolymer was dialyzed against deionized water for 1 week and recovered by lyophilization. The triblock copolymer sample was denoted as $PSS_xPEG_{90}PSS_x$, where the subscripts *x* and 90 were the degree of polymerization of the PSS and PEG blocks, respectively. For example, $PSS_{24}PEG_{90}PSS_{24}$ means a triblock copolymer containing two PSS blocks with 24 sodium styrenesulfonate repeat units for each and 90 of ethylene glycol repeat units for the PEG block.

Solution Preparation

Sample solution was prepared in the following way. Certain amount of $PSS_xPEG_{90}PSS_x$ copolymer was dissolved in pure water to ensure that the sulfonic group concentration $[SO_3^-]$ in the final solution was maintained at 0.002 mol/L. Aluminum chloride was dissolved in 0.1 mol/L hydrochloric acid aqueous solution to the aluminum ion concentration $[Al^{3+}]$ of 0.1 mol/L. The aluminum ion in the acidic solution would exist as a six-fold coordinated ion $[Al(H_2O)_6]^{3+}$, where six water molecules were octahedrally arranged around an aluminum ion [27,28]. Here, we considered this coordinated Al^{3+} as an aluminum ion for simplification. The solution was filtered through a Millipore membrane of pore size of 0.22 μm to remove dust. 2.0 mL of dust-free $PSS_xPEG_{90}PSS_x$ aqueous solution was neutralized by titration with designed amount of dust-free $AlCl_3$ aqueous solution to realize required degree of neutralization (DN) under stirring with a magnetic stirrer for 5 min. DN was defined as the mole ratio of the Al^{3+} ion to the SO_3^- ion in the test solution.

Measurements

^1H NMR spectra were recorded on a Bruker Avance Digital 400MHz NMR spectrometer in D_2O. The molecular weight and polydispersity of the PEG macro-CTA and triblock copolymers were determined with a gel permeation chromatography (GPC, Waters 2410) using aqueous solution of 0.1 M Na_2SO_4 as the eluent (0.6 mL/min)

at 25°C. The calibration curve was established using a set of narrowly distributed poly(ethylene oxide) as the standards.
The solution transmittance T was measured with a Hitachi UV-3010 UV/Vis spectrophotometer at 400 nm and 25°C. The turbidity was calculated from T as (100 - T)/100. The solution was equilibrated for about 5 min prior to measurement.
The zeta potential of the aggregates was measured at 25°C with a Nano-ZS90 Zetasizer (Malvern Co.) equipped with a 22 mW He-Ne laser operating at λ = 633 nm. The apparent hydrodynamic radius R_h was determined with the photon correlation spectroscopy using the same instrument at 90º scattering angle. The CONTIN algorithm was adopted in the Laplace inversion of the autocorrelation function to obtain the size distribution of the aggregates. R_h was evaluated from the Stokes-Einstein equation as $R_h = kT/6\pi\eta D$, where k was the Boltzmann constant, T was the absolute temperature, η was the solution viscosity and D was the apparent diffusion coefficient. The solution was equilibrated for about 5 min before test.
Transmission electron microscopy (TEM) was performed with a FEI-Tecnai 12 operated at acceleration voltage of 120 kV. 5 μL of the $PSS_{42}PEG_{90}PSS_{42}$ solution of DN = 0.3 was dropped onto a copper grid (300 mesh) coated with carbon. Water was allowed to evaporate from the grid at atmospheric pressure and 25°C.

Results and Discussion

Characterization of PSS-b-PEG-b-PSS Triblock Copolymers

In a recent work, we investigated the RAFT polymerization of NaSS using PEG macro-CTA and ACPA as the CTA and initiator, respectively, at 70°C in aqueous solution. The polymerization proceeded following the pseudo first-order kinetics and leading to more than 90% NaSS conversion within 300 min after the 45 min initial induction time when $[CTA]_0/[ACPA]_0$ = 2.5 [26]. In this work, four well-defined PSS-*b*-PEG-*b*-PSS triblock copolymers with different lengths of the PSS block have been synthesized via. the RAFT polymerization following the same procedure as shown in Scheme 1 and characterized with ^{1}H NMR and GPC. The length of PSS block was controlled by the amount of NaSS monomer.

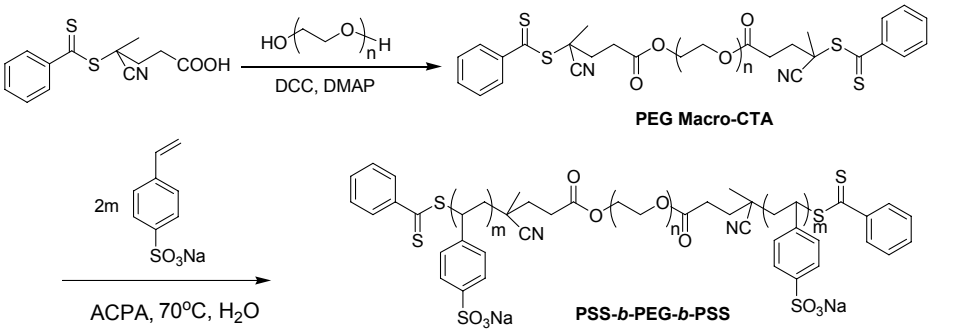

Scheme 1. Synthesis route of the PSS-*b*-PEG-*b*-PSS triblock copolymer using RAFT in aqueous solution

The ^{1}H NMR spectrum of $PSS_{60}PEG_{90}PSS_{60}$ triblock copolymer in D_2O is given in Figure 1 as an example. The total degree of polymerization (DP_{SS}, $DP_{SS} = 2x$) of the PSS block, the conversion of NaSS (Conv%) and molecular weight of PSS-*b*-PEG-*b*-PSS triblock copolymer ($M_{n,NMR}$) can be experimentally determined from the NMR peak area at 1.2-2.0 ppm, which is attributed to the aliphatic -CH-CH_2- protons of the PSS block, and that at 3.6 ppm corresponding to the -CH_2-CH_2O- protons of PEG block.

$$DP_{SS} = (I_{1.2\text{-}2.0})/3/[I_{3.6}/(4 \times 90)] \quad (\mathbf{1})$$

$$Conv\% = DP_{SS}/DP_{SS,cal} \quad (\mathbf{2})$$

$$M_{n,NMR} = DP_{SS} \times M_{NaSS} + M_{CTA} \quad (\mathbf{3})$$

Here, $DP_{SS,cal}$ is the calculated DP according to the ratio of $[NaSS]_0/[CTA]_0$, M_{NaSS} and M_{CTA} are the molecular weight of NaSS monomer and PEG macro-CTA, $I_{1.2\text{-}2.0}$ and $I_{3.6}$ are the integral area of the NMR peaks at 1.2-2.0 and 3.6 ppm, respectively.

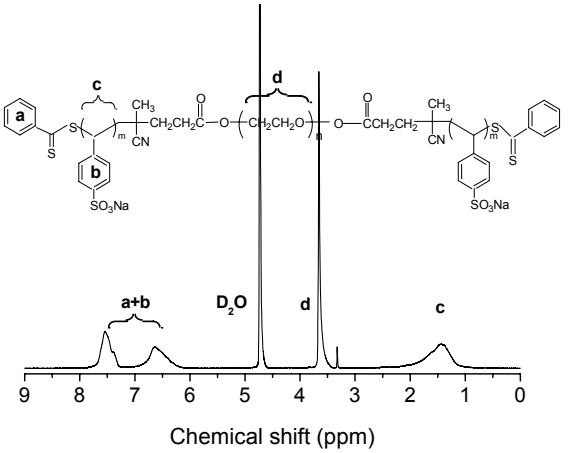

Fig. 1 ^{1}HNMR spectrum of $PSS_{60}PEG_{90}PSS_{60}$ triblock copolymer in D_2O

Figure 2 depicts the GPC traces of the PEG macro-CTA and PSS-*b*-PEG-*b*-PSS triblock copolymers with different lengths of PSS block. All the triblock copolymers exhibit symmetrical a unimodal distribution peak at high molecular weight position compared to that of the PEG macro-CTA, indicating the formation of PSS-*b*-PEG-*b*-PSS triblock copolymer rather than a mixture of PEG macro-CTA and PSS homopolymer. The characterization results of these copolymers with ^{1}H NMR and GPC are listed in Table 1. In the four cases, more than 84% conversion was realized and relatively narrow molecular weight distribution ($1.29 < M_w/M_n < 1.36$) was observed, which indicated that four PSS-*b*-PEG-*b*-PSS triblock copolymers with well-defined structure and narrow molecular weight distribution have been synthesized via. the RAFT polymerization.

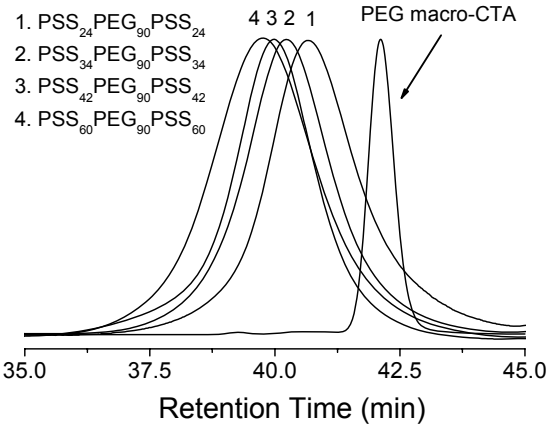

Fig. 2 GPC traces of PEG macro-CTA and PSS-*b*-PEG-*b*-PSS triblock copolymers with different lengths of the PSS blocks

Table 1. Characteristics of PSS-*b*-PEG-*b*-PSS triblock copolymer

Sample	$[NaSS]_0/[CTA]_0$	M_n [a]	M_w [a]	M_w/M_n [a]	DP_{SS} [b]	Conv (%) [b]	$M_{n,NMR}$ [b]
$PSS_{24}PEG_{90}PSS_{24}$	50	12100	16100	1.32	48	96	14600
$PSS_{34}PEG_{90}PSS_{34}$	75	15400	19900	1.29	68	90	18500
$PSS_{42}PEG_{90}PSS_{42}$	100	17400	23000	1.32	84	84	21800
$PSS_{60}PEG_{90}SS_{60}$	125	23800	32300	1.36	120	96	29200

[a] Determined with GPC in aqueous solution of 0.1 M Na_2SO_4 at 0.6 mL/min using PEO standards; [b] Determined from ^1H NMR peak area ratio

Turbidity

Turbidimetric titration with Al^{3+} cations was performed to reveal complexation in the PSS-*b*-PEG-*b*-PSS aqueous solution. Four PSS-*b*-PEG-*b*-PSS triblock copolymers with different PSS block lengths were used in this experiment. Li et al. found that the turbidity of PEO-*b*-PMAA/metal ion mixtures increased with increasing amount of Ba^{2+} or Ca^{2+}, indicating the formation of water insoluble PEO-*b*-PMAA/metal ion aggregates [16]. In our preliminary experiments, we did not observe the turbidity from PSS-*b*-PEG-*b*-PSS/metal ion aqueous solution when titrated with Ba^{2+} or Ca^{2+} cations at all DN values examined, which suggests no water insoluble aggregates appearing in the solution. In contrast, the turbidity of PSS-*b*-PEG-*b*-PSS aqueous solutions increased dramatically with increasing DN when titrated with Al^{3+} cations to neutralize the PSS anion. Two different modes of polyelectrolyte precipitation by multivalent counterion have been investigated in the previous literatures [23, 29-31]. The first mode follows the law of mass action and conforms to the requirement of a constant solubility [23]. For example in the case of PSS with Ca^{2+} or Ba^{2+} system, Ca^{2+} or Ba^{2+} with SO_3^- of the PSS chain associate and adhere to the PSS macromolecular chain.[23]. The first mode explains why we did not observed turbidity in PSS-*b*-PEG-*b*-PSS/Ca^{2+} and PSS-*b*-PEG-*b*-PSS/Ba^{2+} systems. In the

second mode, precipitation or aggregation occurs due to multiple ionic bridging between the multivalent counterion and anion on the polyelectrolyte chain (COO^- for PAA and SO_3^- for PSS) when the degree of neutralization reaches to a critical value (CDN). Above CDN, precipitation of polyelectrolyte occurs and the solution has two phases, and the amount of counterion for precipitating the polyelectrolyte proportional increases with increasing polyelectrolyte concentration [23]. Keller et al. has investigated that precipitation follows the second mode in the case of PSS/Al^{3+} systems, and the threshold value of the Al^{3+} concentration ($[Al^{3+}]_T$) at which precipitation occurs linearly increases with increasing PSS concentration [23].

Figure 3 shows the turbidity of the PSS-*b*-PEG-*b*-PSS/Al^{3+} system as a function of DN at constant [SO_3^-] of 0.002 mol/L. At low DN, the turbidity is almost zero. Whereas, the turbidity increases abruptly to exceed 0.9 and the solution becomes opalescent when the DN changes from 0.3 to 0.4, which indicates the formation of water insoluble PSS-*b*-PEG-*b*-PSS/Al^{3+} aggregates. This can be attributed to the electrostatic combination between the SO_3^- groups in the PSS blocks and Al^{3+} ions. The DN value is about 0.33 at the highest turbidity for each triblock copolymer, which approximately equals to the amount of Al^{3+} required for the complete neutralization of the corresponding negative charges. A larger flocculating aggregation was observed at DN 0.4 to 0.8 which should be attributed to further aggregate of the neutral PSS-*b*-PEG-*b*-PSS/Al^{3+} aggregation for hydrophobic interaction, and resulted in the turbidity slightly decreased. These aggregations are stable and no precipitation was observed for several days. At DN > 0.8, filamentous precipitation was observed and the turbidity sharply decreased due to salt-out effect. The DN value at which turbidity starts to increase is defined as the critical degree of neutralization (CDN).

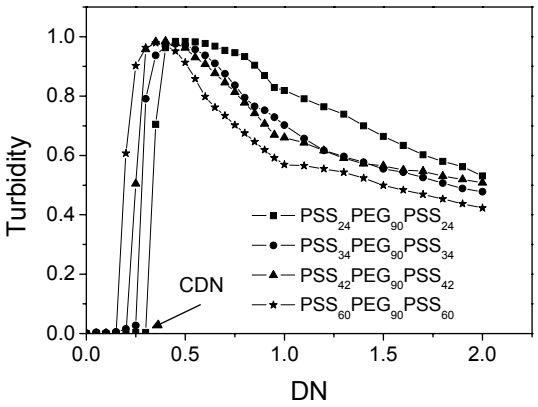

Fig. 3 Turbidity of aqueous solutions of PSS-*b*-PEG-*b*-PSS copolymers with different PSS block lengths as a function of DN

Figure 4 depicts the PSS block length dependence of the CDN, where DP_{SS} equals to 2*x* for the triblock copolymer $PSS_xPEG_{90}PSS_x$. The CDN obviously decreases with increasing DP_{SS}, indicating that appearance of the PSS-*b*-PEG-*b*-PSS/Al^{3+} aggregates strongly depends on the length of the ionic PSS block. The formation of the PSS-*b*-PEG-*b*-PSS/Al^{3+} aggregates is caused by the intra- and intermolecular association of

PSS block. The SO_3^- groups and Al^{3+} caions act as a "sticker" and a cross linking agent to complex with the PSS block. This association is similar and a cross linking agent to complex with the PSS block. This association is similar to that of carboxylic groups and Ca^{2+} ions in partially hydrolyzed poly(acrylamide) (HPAM)/Ca^{2+} system and polymethacrylate (PMA)/Ca^{2+} system [32,33]. There are more associating points at one PSS-*b*-PEG-*b*-PSS chain with longer PSS blocks, leading to a lower CDN. Therefore, long PSS block is favorable for the association of PSS-*b*-PEG-*b*-PSS chains induced by Al^{3+} ions.

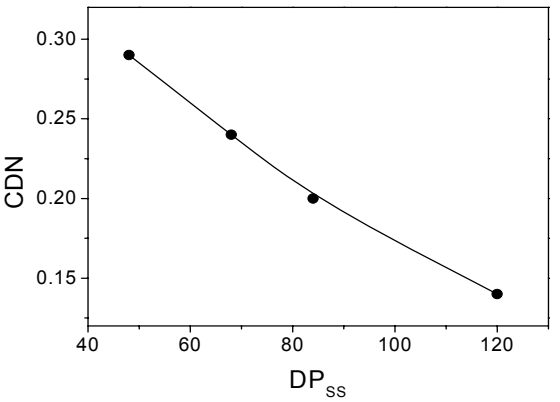

Fig. 4 The critical degree of neutralization CDN varying with the degree of polymerization of the PSS block DP_{SS}

Figure 5 shows turbidity of aqueous solutions of $PSS_{42}PEG_{90}PSS_{42}$ copolymers with different concentration (C_P) as a function of Al^{3+} concentration (a) and plot of Al^{3+} concentration threshold ($[Al^{3+}]_T$) as a function of C_P (b). As shown in Fig. 5a, the turbidity is almost zero at lower $[Al^{3+}]$, whereas, the turbidity increases abruptly and the solution becomes opalescent when the $[Al^{3+}]$ changes to a threshold value $[Al^{3+}]_T$. The value of $[Al^{3+}]_T$ linearly increases with increasing C_P in Fig. 5b which indicates the aggregate behavior of PSS-*b*-PEG-*b*-PSS/Al^{3+} system follows the second mode. The insoluble PSS-*b*-PEG-*b*-PSS /Al^{3+} aggregations are formed by the multiple ionic bridging between trivalent Al^{3+} and monovalent sulfonate group (SO_3^-) on the PSS block in the PSS-*b*-PEG-*b*-PSS macromolecular chain, and are stabilized by the longer hydrophilic PEG block.

Zeta-potential and size of the aggregates

The zeta-potential and hydrodynamic radius of the PSS-*b*-PEG-*b*-PSS/Al^{3+} aggregates were observed as a function of DN and shown in Figure 6. The zeta-potential sharply increases with increasing DN, and then gradually approaches to a constant at -5 mV as DN within 0.4 ~ 2.0. The DN value at the inflexion point of the zeta-potential vs. DN curve is about 0.33, which is consistent with the DN value at the highest turbidity. These results imply that the negative charge of the SO_3^- groups at the PSS-*b*-PEG-*b*-PSS chains is almost neutralized with Al^{3+} cations to form the aggregates. Further

addition of Al^{3+} cations as DN from 0.4 to 2.0 changes the zeta-potential slightly and the excess Al^{3+} cations act as an added salt to affect the stability of the neutral PSS-*b*-PEG-*b*-PSS/Al^{3+} aggregates in aqueous solution due to the salt-out effect [34].

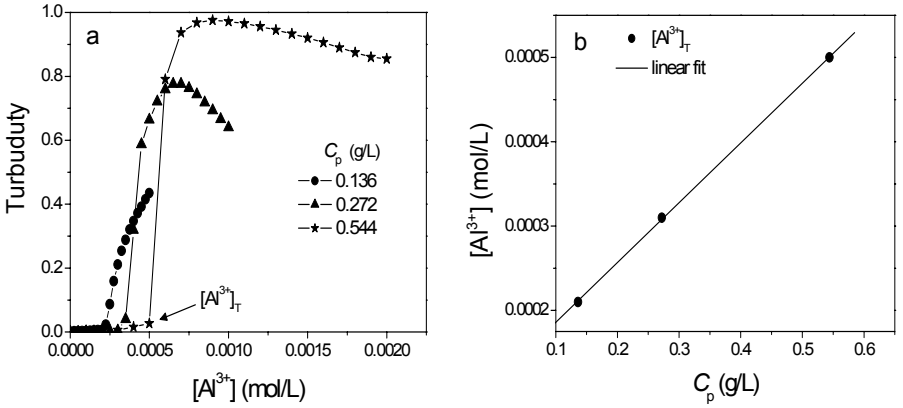

Fig. 5 Turbidity of aqueous solutions of $PSS_{42}PEG_{90}PSS_{42}$ copolymers with different concentration (C_P) as a function of Al^{3+} concentration (a) and plot of Al^{3+} concentration threshold ($[Al^{3+}]_T$) as a function of C_P (b)

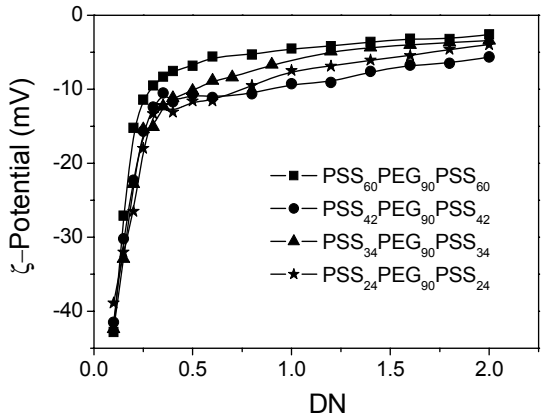

Fig. 6 Variation of ζ-potential of the PSS-*b*-PEG-*b*-PSS/Al^{3+} aggregates as a function of DN

The hydrodynamic radius of the aggregates was determined with dynamic light scattering (DLS). Figure 7 illustrates the intensity autocorrelation function (a) and intensity-averaged hydrodynamic radius R_h distribution (b) of the $PSS_{60}PEG_{90}PSS_{60}/Al^{3+}$ aggregates at different DN as an example. Two relaxation modes can be observed from the intensity autocorrelation curve of DN = 0.2. The fast mode appears to correspond to the diffusion of shrinking coil with R_h = 6.6 ± 0.6 nm and the slow one to the aggregates with R_h = 58.6 ± 11.2 nm. These aggregates are

formed due to the electrostatic association of the SO_3^- groups at the PSS blocks with the Al^{3+} ions. When DN is at 0.3 ~ 0.8, only one relaxation mode can be observed from the intensity autocorrelation curve. The R_h distribution corresponding to the shrinking coil disappears and another peak appears at higher R_h for the larger interchain aggregates (Figure 7b), which suggests the transition from the shrinking coil to the interchain association induced by binding more Al^{3+} cations. The R_h value increases steeply with increasing DN when DN ranges from 0.3 to 0.8 due to the hydrophobic interaction among the neutralized triblock copolymers, which is enhanced by the salt out effect of the excessive Al^{3+} cations. When DN > 0.8, two R_h distribution peaks appear corresponding to larger aggregates (400 ~ 700 nm) and precipitates (> 2000 nm), respectively.

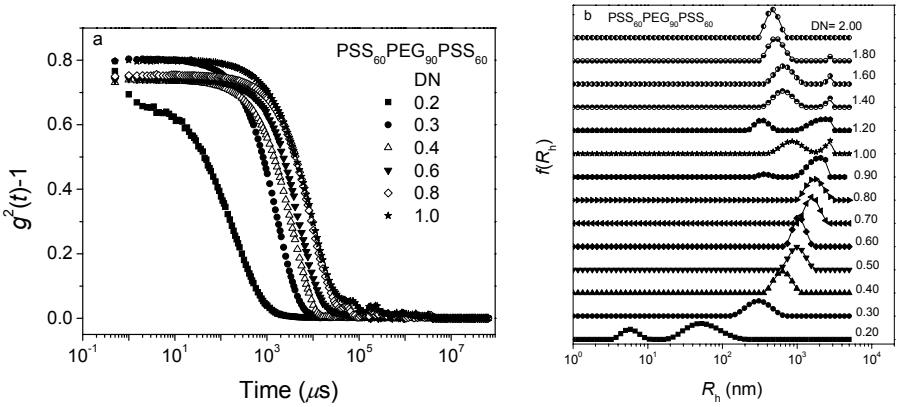

Fig. 7 The intensity autocorrelation function (a) and intensity-average hydrodynamic radius Rh distribution (b) of the $PSS_{60}PEG_{90}PSS_{60}$/Al3+ aggregates at different DN

Similar intensity autocorrelation curves were obtained for the $PSS_{42}PEG_{90}PSS_{42}/Al^{3+}$, $PSS_{34}PEG_{90}PSS_{34}/Al^{3+}$ and $PSS_{24}PEG_{90}PSS_{24}/Al^{3+}$ systems. Figure 8 demonstrates the intensity averaged R_h of the PSS-*b*-PEG-*b*-PSS/Al^{3+} aggregates as a function of DN. The dominant R_h was adopted in this figure when there appeared two R_h distribution peaks. At DN = 0.25, R_h is 218, 157, 172, and 124 nm for the $PSS_{60}PEG_{90}PSS_{60}/Al^{3+}$, $PSS_{42}PEG_{90}PSS_{42}/Al^{3+}$, $PSS_{34}PEG_{90}PSS_{34}/Al^{3+}$, and $PSS_{24}PEG_{90}PSS_{24}/Al^{3+}$, respectively. At DN = 0.3, R_h is 319, 190, 168, and 139 nm, respectively. It seems that the aggregate size of the PSS-*b*-PEG-*b*-PSS triblock copolymers associated by Al^{3+} ions increases with the PSS block length at DN close to 0.3. At DN 0.4 to 0.8, further aggregate of the neutral PSS-*b*-PEG-*b*-PSS/Al^{3+} aggregation for hydrophobic interaction gave rise to form larger flocculating aggregation and R_h increased. Further increased DN above 0.8, precipitation occurred for salt-out effect and resulted in R_h erratically decreased. The scattered data suggest the difficulty in determining R_h for the large hydrophobic aggregates.

The aggregates of PSS-*b*-PEG-*b*-PSS/Al^{3+} with different DN were also observed with a TEM. A typical TEM micrograph of the $PSS_{42}PEG_{90}PSS_{42}/Al^{3+}$ aggregates at DN = 0.3 is presented in Figure 9. It is clearly that the aggregates are close to spherical shape with an average diameter of about 100 nm, which agrees well with the DLS result.

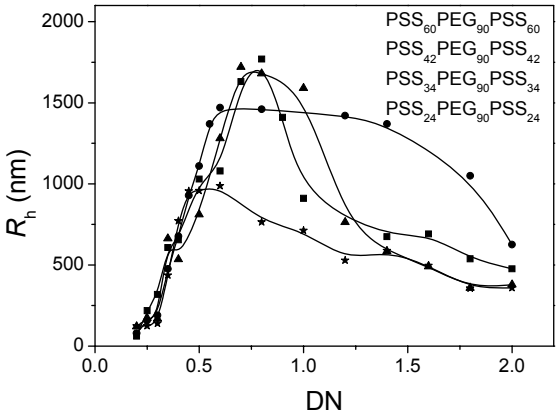

Fig. 8 The intensity average R_h of the PSS-*b*-PEG-*b*-PSS/Al^{3+} aggregates as a function of DN

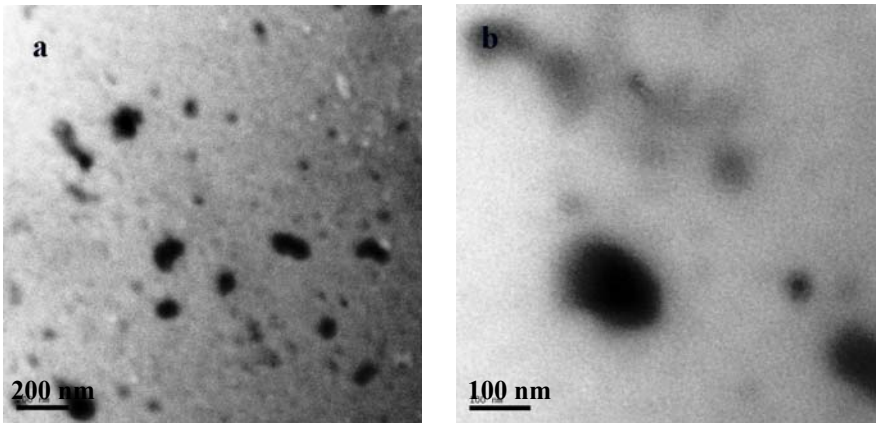

Fig. 9 TEM micrographs of the $PSS_{42}PEG_{90}PSS_{42}/Al^{3+}$ aggregates at DN = 0.3

Conclusions

Water soluble triblock copolymer PSS-*b*-PEG-*b*-PSS with well-defined structure was synthesized via RAFT polymerization and associated with Al^{3+} cations in aqueous solution. The aggregate formation was observed with turbidity titration, zeta-potential, dynamic light scattering, and TEM. The triblock copolymer with longer PSS block was found to be easier to form the aggregates and the zeta-potential of the aggregates approached to zero when neutralized by Al^{3+}. The aggregate size for the PSS-*b*-PEG-*b*-PSS copolymers completely neutralized by Al^{3+} (i.e., DN = 0.33) increased with increasing the PSS block length. The transition from the intrachain aggregate with small size to the interchain aggregate with large size was found at DN of about 0.33. Further increase in DN up to 0.8 induced larger aggregates due to the added salt effect on neutralized copolymers.

Acknowledgements. The authors are grateful to the NSF of China (20534020 and 50773024) for the sponsorship to this work.

References

1. Alvarez-Lorenzo C, Barreiro-Iglesias R, Concheiro A, Iourtchenko L, Alakhov V, Bromberg L, Temchenko M, Deshmukh S, Hatton TA (2005) Langmuir 21:5142
2. Kabanov AV, Kabanov VA (1998) Adv Drug Delivery Rev 30:49
3. Rungsardthong U, Deshpande M, Bailey L, Vamvakaki M, Armes SP, Garnett MC, Stolnik S (2001) J Control Release 73:359
4. Auguste DT, Armes SP, Brzezinska KR, Deming TJ, Kohn J, Prud'homme RK (2006) Biomaterials 27:259
5. Giacomelli C, Schmidt V, Borsali R (2007) Macromolecules 40:2148
6. Karanikolopoulos N, Pitsikalis M, Hadjichristidis N, Georgikopoulou K, Calogeropoulou T, Dunlap JR (2007) Langmuir 23:4214
7. Cölfen H, Antonietti M (1998) Langmuir 14:582
8. Cölfen H, Qi LM (2001) Chem Eur J 7:106
9. Guo XH, Yu SH (2007) Cryst Growth Des 7:354
10. Qi LM, Li J, Ma JM (2002) Adv Mater 14:300
11. Yu SH, Cölfen H, Antonietti M (2003) J Phys Chem B 107:7396
12. Guillemet B, Faatz M, Grohn F, Wegner G, Gnanou Y (2006) Langmuir 22:1875
13. Qi LM, Cölfen H, Antonietti M (2001) Nano Letters 1:61
14. Bronstein LM, Sidorov SN, Gourkova AY, Valetsky PM, Hartmann J, Breulmann M, Cölfen H, Antonietti M (1998) Inorg Chim Acta 280:348
15. Cölfen H (2001) Macromol Rapid Comm 22:219
16. Li Y, Gong YK, Nakashima K, Murata Y (2002) Langmuir 18:6727
17. Li Y, Ikeda S, Nakashima K, Nakamura H (2003) Colloid Polym Sci 281:562
18. Nishiyama N, Yokoyama M, Aoyagi T, Okano T, Sakurai Y, Kataoka K (1999) Langmuir 15:377
19. Yokoyama M, Okano T, Sakurai Y, Suwa S, Kataoka K (1996) J Control Release 39:351
20. Harada A, Kataoka K (1998) Macromolecules 31:288
21. Harada A, Kataoka K (1999) Langmuir 15:4208
22. Harada A, Kataoka K (1999) J Am Chem Soc 121:9241
23. Narh KA, Keller A (1993) J Polym Sci Part B: Polym Phys 31:231
24. Jan JS, Breedveld V (2008) Macromolecules 41: 6517
25. Dubois E, Boué F (2001) Macromolecules 34: 3684
26. Peng ZP, Wang D, Liu XX, Tong Z (2007) J Polym Sci Part A: Polym Chem 45:3698
27. Ohtaki H, Radnai T (1993) Chem Rev 93:1157
28. Ikeda T, Hirata M, Kimura T (2003) J Chem Phys 119:12386
29. Michaeli I (1960) J Polym Sci 48: 291
30. Ikegami A, Imai N (1962) J Polym Sci 56: 133
31. Schweins R, Huber K (2001) Eur Phys J E 5: 117
32. Peng S, Wu C (1999) Macromolecules 32:585
33. Ikeda Y, Beer M, Schmidt M, Huber K (1998) Macromolecules 31:728
34. Yang YY, Zeng F, Tong Z, Liu XX, Wu SZ (2001) J Polym Sci Part B: Polym Phys 39:901